

# Supplementary information for “Volatile metal emissions from volcanic degassing and lava-seawater interactions at Kīlauea Volcano, Hawai’i”

## Contents

<b>Supplementary Note 1: Sampling and analysis</b> .....	<b>2</b>
S1.1 Diagrams of sampling instruments .....	2
S1.2 Sampling platforms .....	3
S1.3 Summary of samples .....	4
<b>Supplementary Note 2: Multi-GAS data</b> .....	<b>6</b>
<b>Supplementary Note 3: SO<sub>2</sub> emission rate measurements</b> .....	<b>8</b>
<b>Supplementary Note 4: Ash correction figures</b> .....	<b>8</b>
<b>Supplementary Note 5: Calculating emanation coefficients for other volcanoes</b> .....	<b>9</b>
<b>Supplementary Note 6: Speciation modelling</b> .....	<b>10</b>
S6.1 Methods for determining speciation .....	10
S6.2 Data quality in HSC Chemistry.....	10
S6.3 The compositional discontinuity .....	10
S6.4 Simple cooling model for magmatic gas – air mixture .....	13
S6.5 Speciation of volatile trace elements in detail (figures) .....	14
S6.6 Addition of [HCl] to plume .....	16
<b>Supplementary Note 7: Error propagation</b> .....	<b>18</b>
<b>Supplementary Note 8: Comparing size-segregated PM concentrations between Kīlauea’s summit plume in 2008 and the LERZ eruption in 2018</b> .....	<b>20</b>
<b>Supplementary Note 9: Estimating laze plume HCl and trace metal/metalloid emission rates</b> .....	<b>22</b>
<b>Summary of supplementary data</b> .....	<b>24</b>
Supplementary Data file 1 .....	24
Supplementary Data file 2.....	24
<b>References</b> .....	<b>25</b>

## Supplementary Note 1: Sampling and analysis

### S1.1 Diagrams of sampling instruments

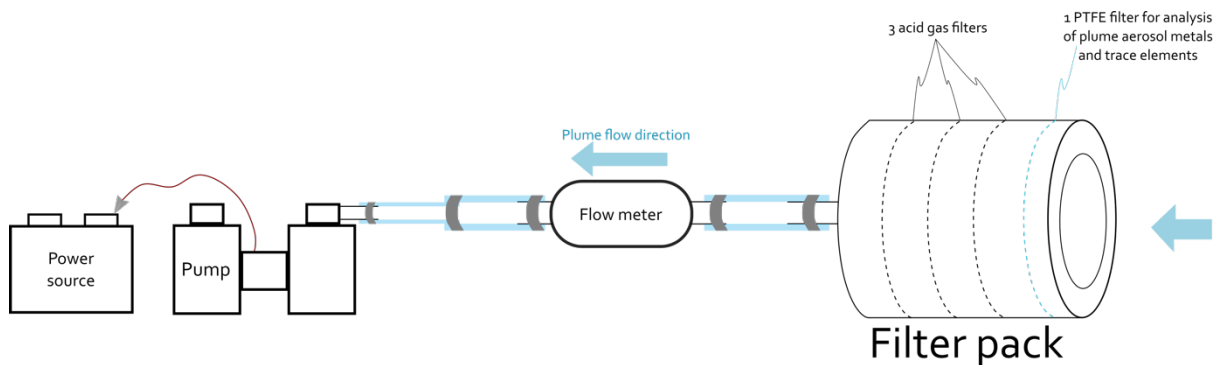


**Figure S1.** Schematic diagram of filter pack used to simultaneously measure gas and particulate compositions of the magmatic and laze plumes.

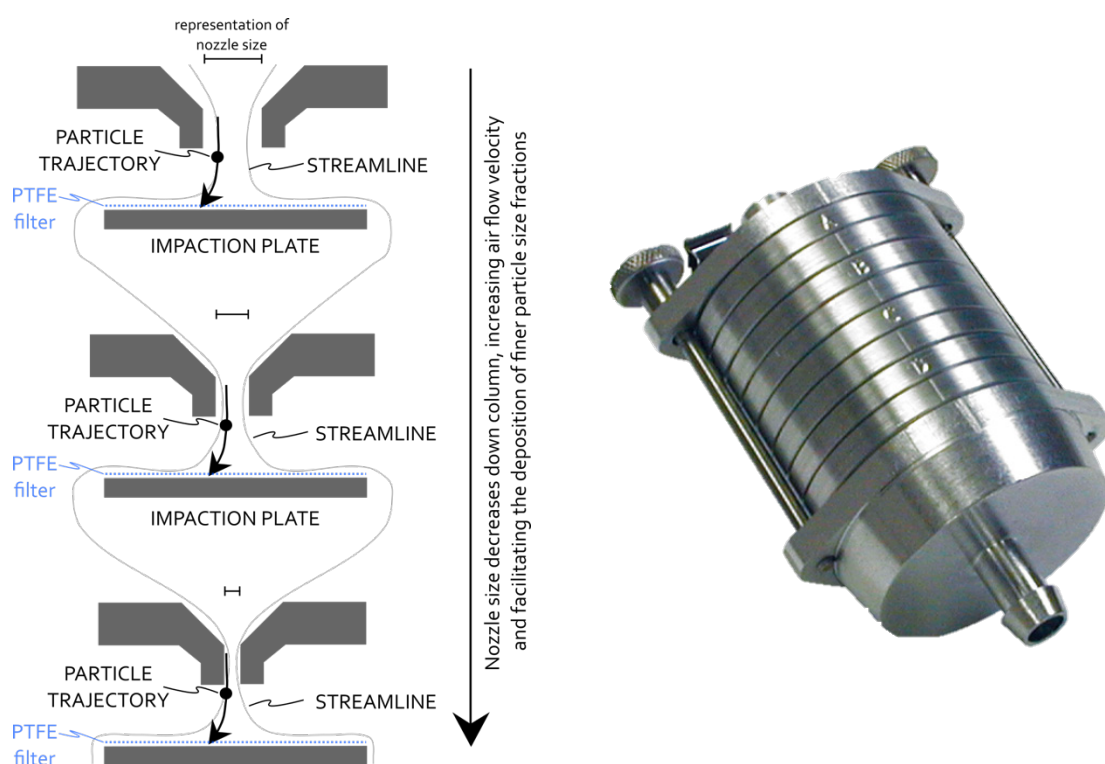


**Figure S2. Left:** Schematic of cascade impactor. Description of cascade impactor mechanism in Methods of main text. **Right:** Outside view of SKC Ltd Sioutas Personal Cascade Impactor, with stages A-D visible, the after-stage is located below stage D. Photo: SKC Ltd. The Sioutas personal cascade impactor has a length of 8.6 cm and a diameter of 5.5 cm.

## S1.2 Sampling platforms

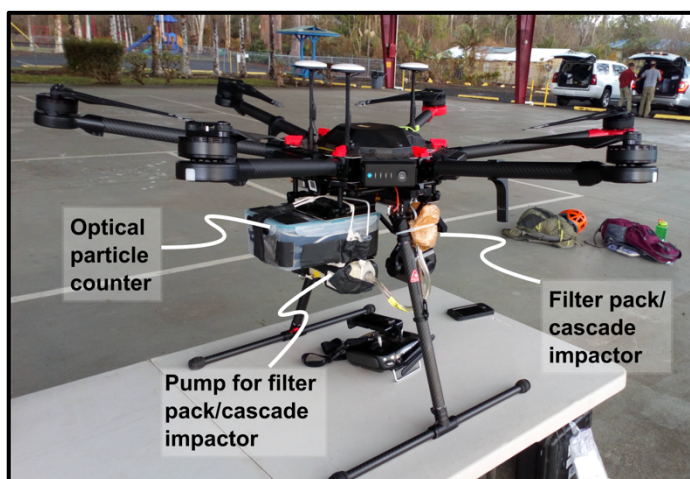


**Figure S3.** DJI Matrice 600 Pro UAS used to fly filter packs or cascade impactors into the Fissure 8 and laze plumes – owned and operated by the United States Geological Survey. Photo: Rachel Whitty.

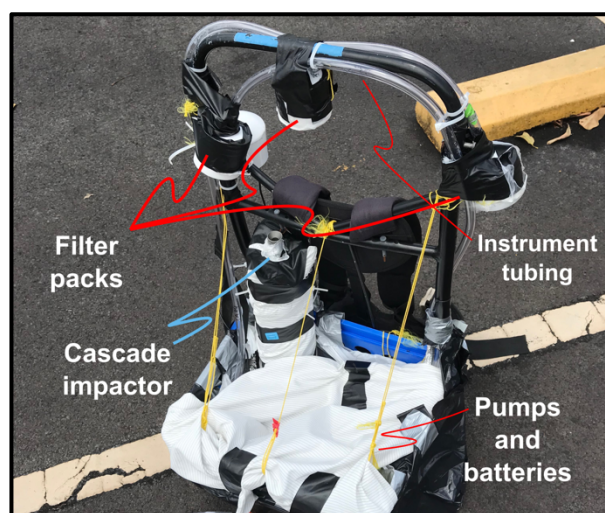


**Figure S4.** Backframe used to carry instruments to near-source ground sampling sites. This allowed a quick 'drop-and-go' approach to limit exposure to high concentrations of SO<sub>2</sub>. Photo: Emily Mason.

### S1.3 Summary of samples

**Table S1.** Samples taken at Fissure 8 and the ocean entry. FP = filter packs; SKC = sioutas cascade impactor. UAS = unoccupied aircraft system. Flow rate accuracies are  $\pm 5\%$  for UAS samples and  $\pm 10\%$  for ground-based samples. Sampling duration is 'time in plume' as determined by multi-GAS SO<sub>2</sub> concentrations (Supplementary Note 2) and visual identification on video, for the ground based and UAS samples, respectively. The local time gives the full time that the pump was running and the sample was exposed to the atmosphere.

Sample name	Location	Date - start to end time (local)	Mean flow rate (L min <sup>-1</sup> )	Sampling duration (min) <sup>1</sup>	Sampling platform	Included/excluded (with reasons)?
<b>Fissure 8</b>						
FP_8_1	~300 m above vent (UAS flown from Leilani Estates community centre)	24/07/18 10:17 to 10:47	9.3	23	UAS (Matrice 600 Pro)	Excluded (saturated)
FP_8_2	Tephra field	24/07/18 15:50 to 18:47	14.85	177	Ground-based	Excluded (saturated and affected by fumarolic gases)
FP_8_5	Tephra field	31/07/18 13:11 to 13:27	22.0	16	Ground-based	Included
FP_8_6	Tephra field	31/07/18 13:27 to 15:06	21.2	99	Ground-based	Included
SKC_8_2	~300 m above vent (flown from Leilani Estates community centre)	29/07/18 09:42 to 10:41	9.0	35	UAS (Matrice 600 Pro)	n/a
<b>Ocean entry</b>						
FP_9_1	~100-150 m above sea level (flown from Mackenzie State Recreation Area)	29/07/18 15:40 to 16:31	9.5	51	UAS (Matrice 600 Pro)	Excluded (saturated and only sampled the very dilute and distal laze plume)

<b>FP_9_2</b>	~100-150 m above sea level (flown from Isaac Hale Park)	02/08/18 10:06 to 10:52	10.0	15	UAS (Matrice 600 Pro)	Included
<b>SKC_9_2</b>	~100-150 m above sea level (flown from Isaac Hale Park)	02/08/18 12:06 to 13:21	9.0	40	UAS (Matrice 600 Pro)	n/a

Typically, gas filters are assessed to be saturated when the final filter contains non-negligible concentrations (<10% total concentrations of species, e.g., <sup>1</sup>). We assess this for the samples considered here in **Figure S5**.

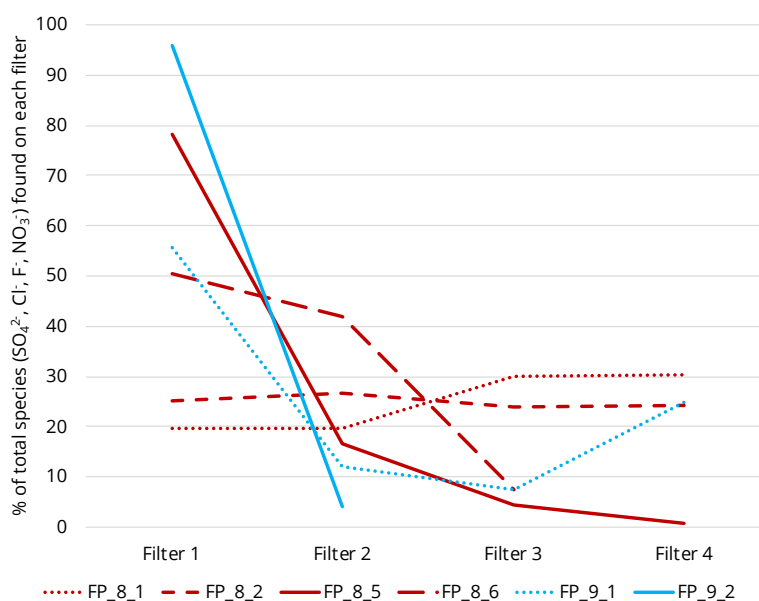


**Figure S5. Assessing whether filter pack samples were saturated.** Total percentages of all anions measured on each filter are shown as a percentage of the total concentrations of all species across all filters in each sample. Red lines denote samples collected at Fissure 8 (only FP\_8\_1 was collected using a UAS, all others were ground-based), blue lines denote samples collected from the laze plume. All samples contained 4 filters, except FP\_8\_6, collected at Fissure 8, which contained 3 filters, and FP\_9\_2, both collected from the laze plume using a UAS, which contained 2 filters. Samples FP\_8\_1, FP\_8\_2 and FP\_9\_1 are excluded from further analysis of their gas compositions as their high concentrations of the final filter show that they are likely to be saturated.

Gas filters from several samples were found to be saturated (**Supplementary Figure S5**). However, the concentrations of particulate matter measured on the first (PTFE) filter may still be used, particularly to calculate trace element ratios, and are therefore included in enrichment factor and weighted ash fraction calculations (**Supplementary Data S10**).

## Supplementary Note 2: Multi-GAS data

The multi-GAS was used primarily to estimate the time in plume during the ground-based filter pack magmatic plume sampling (as described in **Methods** in the main text), but an CO<sub>2</sub>/SO<sub>2</sub> ratio was also calculated for 31 July 2018. To isolate the magmatic component in the periodically grounding plume (**Supplementary Figure S6B**), the CO<sub>2</sub>/SO<sub>2</sub> ratio was calculated using only the SO<sub>2</sub> peaks to give a weighted average of  $0.38 \pm 0.08$ . If the entire time series is used the calculated ratio is almost identical,  $0.38 \pm 0.10$  but with a lower R<sup>2</sup> of 0.1798.

Multi-GAS measurements were also made on 24 July 2018, however gas compositions indicate a high contribution of local scrubbed fumarolic gases as the CO<sub>2</sub> and H<sub>2</sub>O concentrations are strongly coupled (R<sup>2</sup>=0.646 for the whole time series in **Supplementary Figure S6A**), but decoupled from SO<sub>2</sub> (R<sup>2</sup>=0.1). As a result any filter pack samples taken on 24 July 2018 have been discarded as they are not believed to represent the magmatic plume composition exclusively.

**Table S2.** Ground-based multi-GAS gas compositions and ratios measured during filter pack sampling. CO<sub>2</sub>/SO<sub>2</sub> ratios on the same given day are measured from different peaks in the signal, corresponding to pulses of plume that would ground over to the instrument. N = number of measurements contributing to ratio.

Date	CO <sub>2</sub> /SO <sub>2</sub>	Error (±)	SO <sub>2</sub> max	R <sup>2</sup>	N	Notes
31/07/2018	0.41	0.10	117.79	0.871	203	
31/07/2018	0.36	0.11	129.84	0.573	579	
31/07/2018	0.38	0.05	170.49	0.904	377	
31/07/2018	0.96	0.27	40.41	0.760	290	Excluded from average due to low SO <sub>2</sub> max
Weighted average	0.38	0.08				

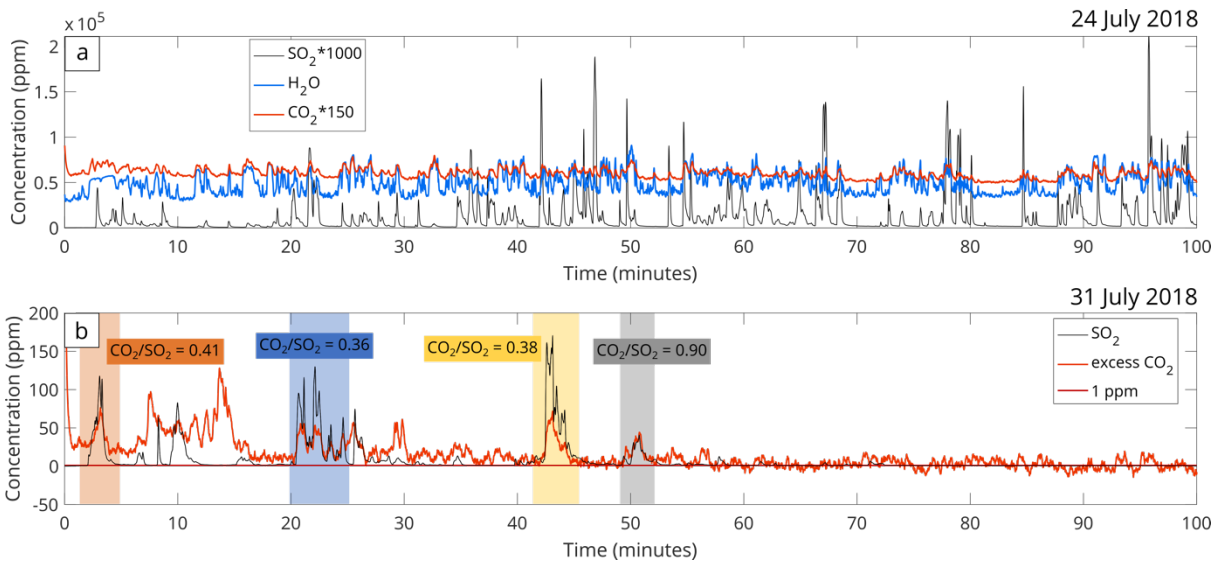


**Figure S6. a:** Time series of  $\text{CO}_2$ ,  $\text{SO}_2$ , and  $\text{H}_2\text{O}$  concentrations measured on the tephra field behind Fissure 8 on 24/07/18. **b:** Timeseries of  $\text{SO}_2$  and  $\text{CO}_2$  concentrations measured on the tephra field behind Fissure 8 on 31/07/18, concurrently with two non-saturated ground-based filter packs (8\_5 and 8\_6). 1 ppm plume marker concentration used for time in plume calculations shown as a solid straight line.

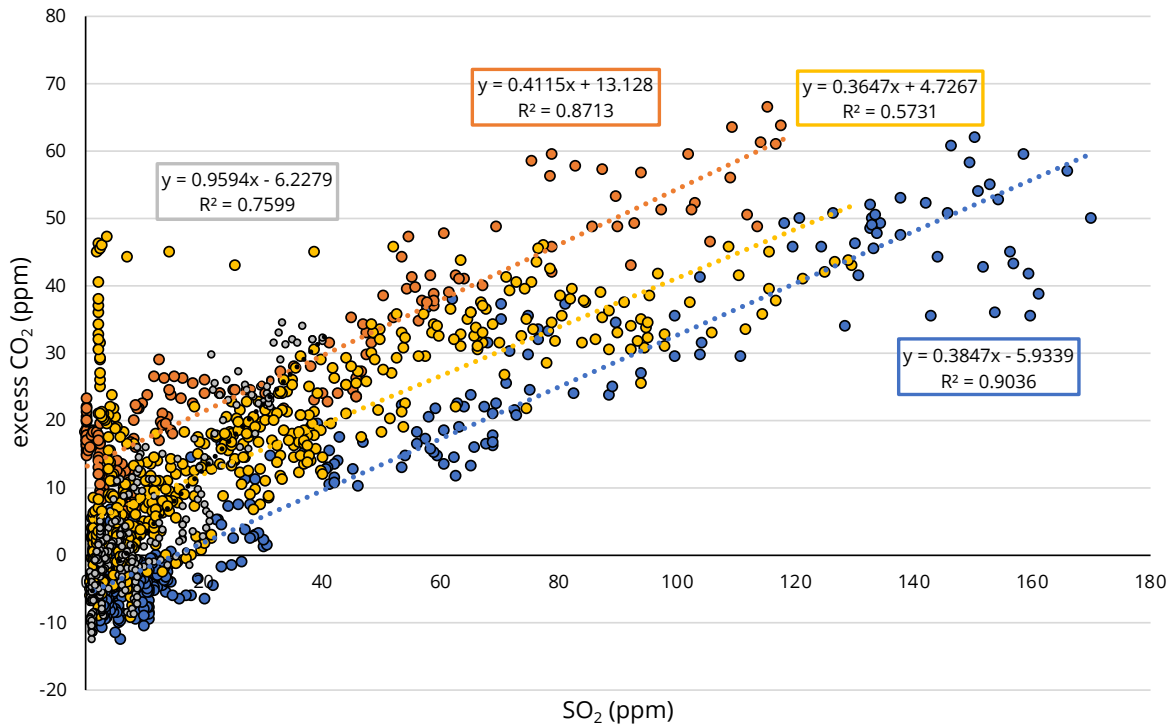


**Figure S7.**  $\text{CO}_2$ - $\text{SO}_2$  plot from multi-GAS sampling of the grounding magmatic plume on 31/07/18. Different colours represent different regions of the gas concentration time series used to calculate the  $\text{CO}_2/\text{SO}_2$  ratios in Supplementary Table S3.

### Supplementary Note 3: SO<sub>2</sub> emission rate measurements

For details of SO<sub>2</sub> emission rate measurement methodology, see **Methods** in the main text.

**Table S3.** SO<sub>2</sub> emissions, measured using a PiSpec instrument on the 31/07/18 (01/08/18 UTC). The 4 measurement periods are shown before. Further details can be found in Methods.

Start Time (UTC)	End Time	Plume Speed (m s <sup>-1</sup> )	Emission rate (kg s <sup>-1</sup> )
01:23:25	01:41:00	6.5	630 (54,000 t day <sup>-1</sup> )
01:45:03	02:00:03	6.5	320 (27,000 t day <sup>-1</sup> )
02:01:53	02:11:26	6.5	410 (36,000 t day <sup>-1</sup> )
02:24:25	02:38:35	6.5	400 (34,000 t day <sup>-1</sup> )

### Supplementary Note 4: Ash correction figures

For details of ash correction methodology, see **Methods** in main text.

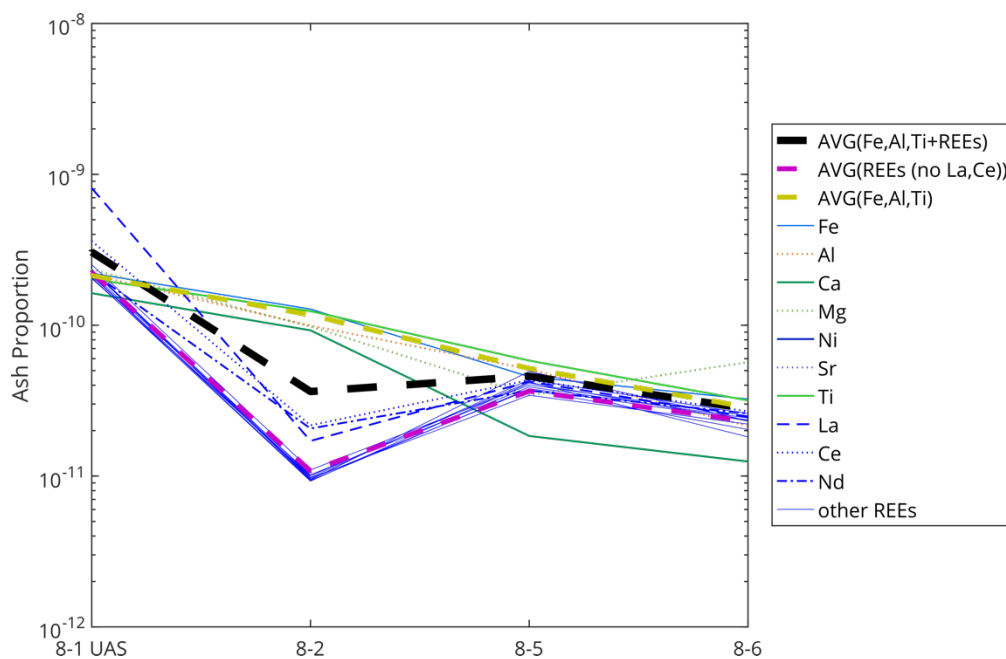


**Figure S8.** Ash proportions calculated based on different elements as averages or individually. AVG = average. The dashed black line represents the ash proportion used in this study (Fe, Al, Ti, +REEs, excluding La and Ce).

## Supplementary Note 5: Calculating emanation coefficients for other volcanoes

Emanation coefficients for the compilation in Figure 5 in the main text are either:

- calculated by the same method as for Kīlauea 2018 (see Methods in the main text), or
- reported directly in the paper (e.g. using the composition of degassed and undegassed melts e.g. Wieser et al.<sup>2</sup>, or  $\varepsilon_{pb}$  e.g. Gauthier et al.<sup>3</sup>).

For those that are calculated, a value of  $S_{degassed}$  is required. The table below describes the accepted  $S_{degassed}$  values for the datasets for which emanation coefficients were calculated.

**Table S4.**  $S_{degassed}$  values accepted for calculation of emanation coefficients for **Figure 5** in the main text (data for figure in **Supplementary Data S16**).

<b>Dataset</b> <small>aerosol dataset reference</small>	<b>Accepted <math>S_{degassed}</math> value (ppm)</b> <small>reference</small>
Etna 2001 <sup>4</sup>	2800 <sup>5</sup>
Stromboli 1993-97 <sup>6</sup>	1600 <sup>7</sup>
Masaya 2000-01 <sup>8</sup>	190 <sup>9</sup>
Ambrym 2007-08 <sup>10</sup>	2050 <sup>10</sup>
Erta Ale 2011 <sup>11</sup>	440 <sup>9</sup>

## Supplementary Note 6: Speciation modelling

### S6.1 Methods for determining speciation

Previous studies of volcanic emissions have taken different approaches to determine or infer speciation. These include thermodynamic models (e.g. HSC chemistry<sup>12-14</sup>, GASWORKS/SOLVGAS<sup>15</sup> and others<sup>16</sup>), cluster analysis<sup>4</sup>, comparison of correlation coefficients between trace elements and different ligands<sup>8</sup> and studies of mineral species in sublimates<sup>11</sup>. We did not have enough source samples of either Fissure 8 or the ocean entry plume to meaningfully assess the speciation using either cluster analysis or correlation coefficients.

### S6.2 Data quality in HSC Chemistry

In HSC Chemistry, a compilation of literature data is used to calculate the equilibrium composition of mixtures of phases and species. For each species, the literature data is only valid within a certain temperature range, and HSC Chemistry will extrapolate the stability and concentration of species beyond this range if these species are not removed from the model. While some extrapolation may be acceptable, large extrapolations may cause errors. We removed all species for which their presence at high magmatic temperatures would result in a large extrapolation beyond the available temperature range. We have accepted a small amount of extrapolation if the upper temperature limit is close to our considered temperatures of 1016–1145°C, i.e., if the upper temperature limit is ~800°C or higher.

### S6.3 The compositional discontinuity

The extent of atmospheric mixing at which the compositional discontinuity observed in **Figure 6a** of the main paper, and by others<sup>13,17</sup> occurs is dependent on the bulk elemental oxygen in the plume at the point of degassing. An average arc composition and the Kīlauea composition used in speciation modelling in this study are compared in **Supplementary Table S5** and **Supplementary Figure S9**. The higher bulk elemental oxygen content of an average arc plume means that the compositional discontinuity occurs with a lower extent of mixing than in the Kīlauea magmatic

plume. **Supplementary Figure S10** shows the lack of temperature dependence of the compositional discontinuity for the Kīlauean magmatic plume composition. Using a typical arc plume composition, Martin *et al.*<sup>13</sup> observed a CD at ~ 5.7 mol% air ( $V_A/V_M \sim 0.06$ ). For a Kīlauea plume composition (**Supplementary Table S6**), the CD occurs at ~ 15% air ( $V_A/V_M \sim 0.16$ , **Supplementary Figure S12**), because of the higher concentration of reduced species in the Kīlauea plume at the point of emission compared to arc volcanoes.

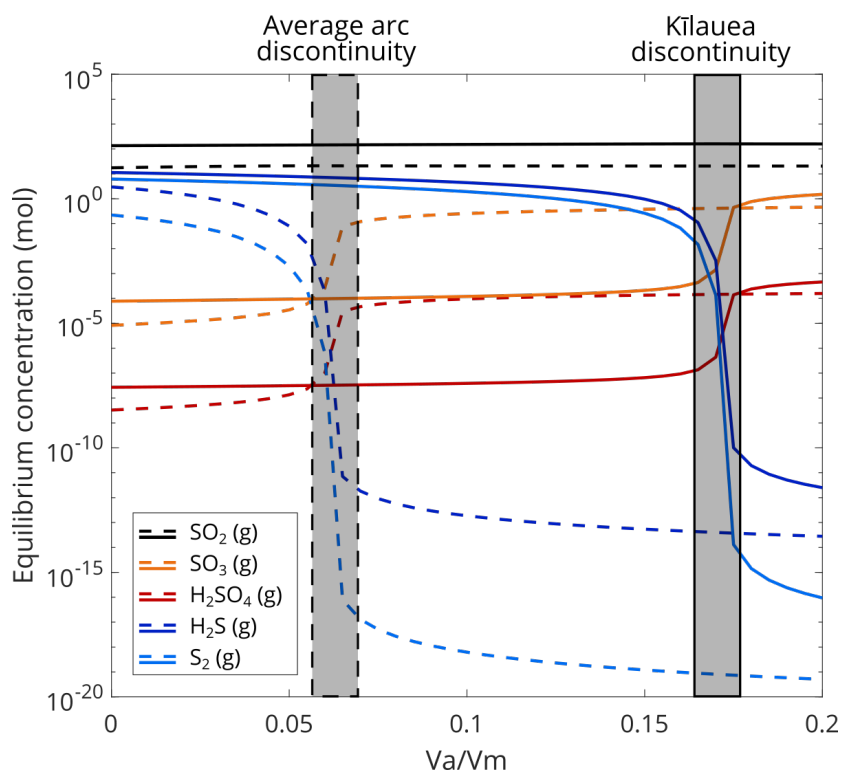


**Figure S9.** Comparison of the amount of atmospheric mixing required to reach the compositional discontinuity in average arc gases (as in Martin *et al.*, 2006) after degassing vs Kīlauea 2018 gases.

**Table S5.** Input data (major gas species only) used for comparison between average arc<sup>13</sup> and compiled Kīlauea data<sup>18,19</sup> for **Supplementary Figure S9**. Full details of inputs for 2018 modelling in main supplement text.

Magmatic gas	Mole fraction	
	Arc average	Kilauea
H <sub>2</sub> O	0.919	0.803
CO <sub>2</sub>	0.046	0.035
SO <sub>2</sub>	0.014	0.137
H <sub>2</sub> S	0.0067	0.012
H <sub>2</sub>	0.0054	0.0094
CO	0.0003	0.0006
HF	0.0006	0.0018
HCl	0.0076	0.0016
HBr	0.000017	0.000004
<b>Bulk O %</b>	<b>0.8533</b>	<b>0.7728</b>

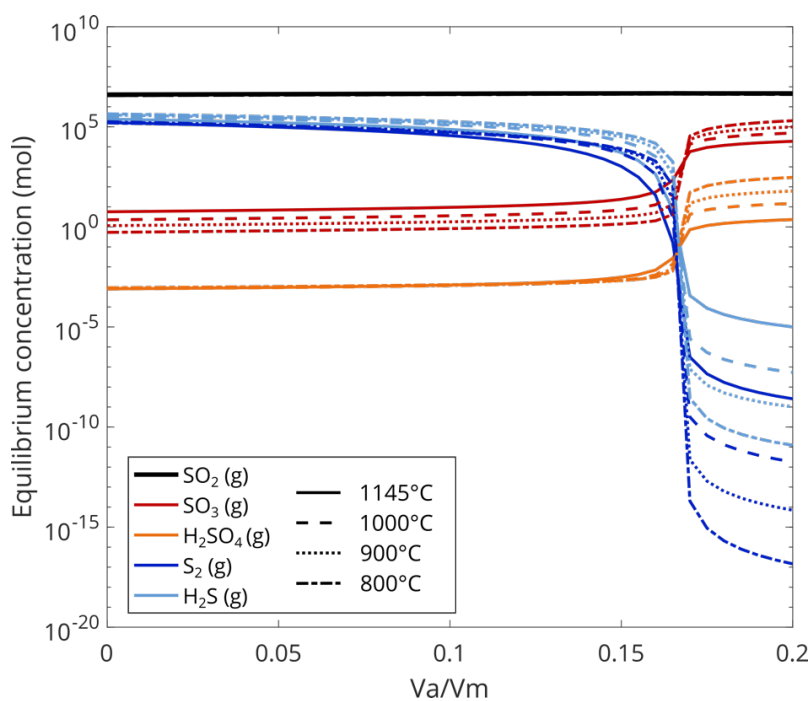


**Figure S10.** The effect of temperature on the extent of atmospheric mixing required to reach the compositional discontinuity. Input data is Kilauea 2018, **Supplementary Data S20**.

#### S6.4 Simple cooling model for magmatic gas – air mixture

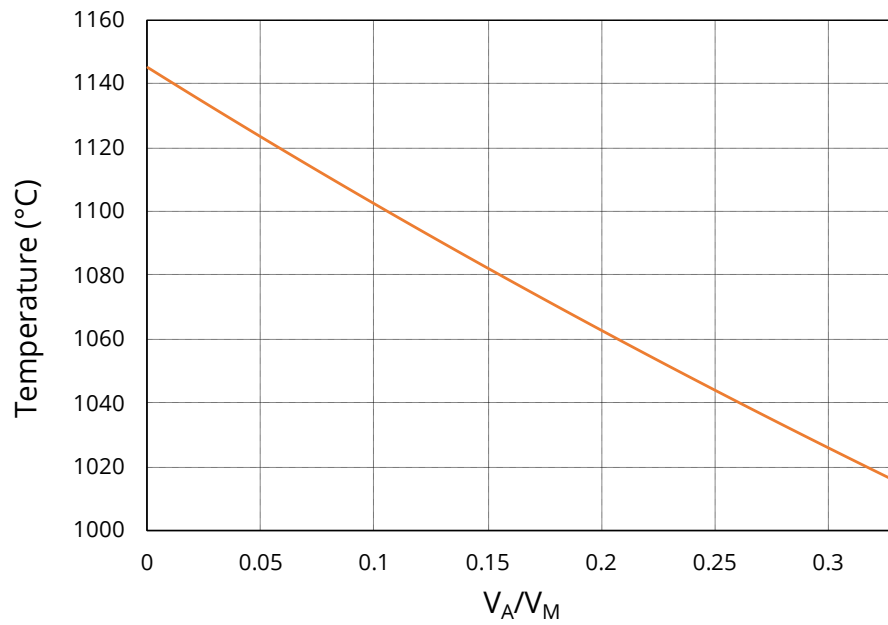


**Figure S11. The effect of mixing air (N<sub>2</sub>, O<sub>2</sub>, Ar gases) into magmatic gases (simplified as H<sub>2</sub>O gas).** Orange line is the modelled output temperature (°C) at increasing degrees of mixing ( $V_A/V_M$ ). See Methods in main text for more detail of model calculations.

## S6.5 Speciation of volatile trace elements in detail (figures)

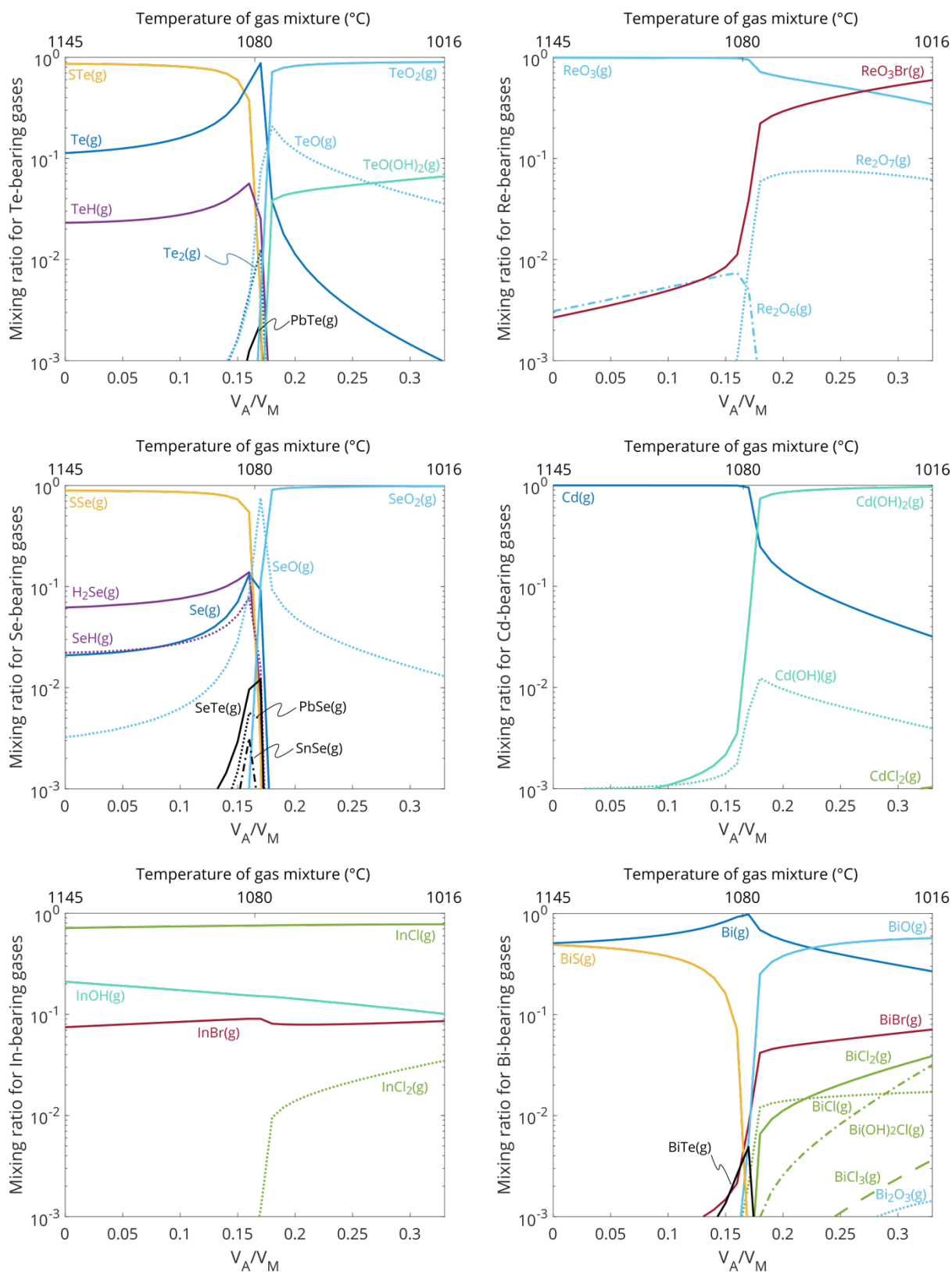


**Figure S12a:** Figures showing the speciation of volatile trace elements in the magmatic plume (original HCl(g) concentration) during oxidation and cooling. Lines depict the mixing ratios for species bearing the elements in question. Mixing ratios are molar ratios, corrected for the amount of the element in question in each species.

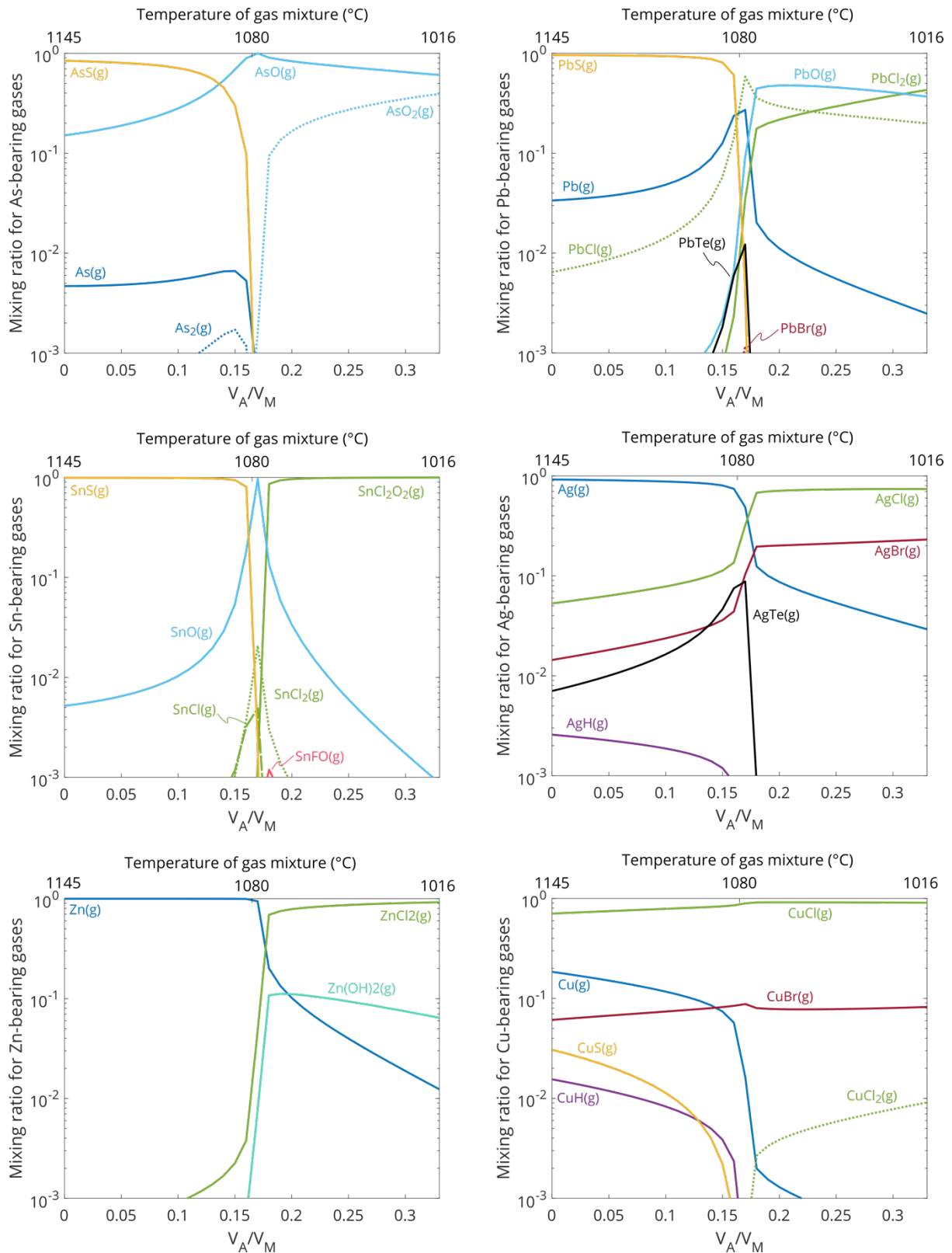


**Figure S12b:** Figures showing the speciation of volatile trace elements in the magmatic plume (original  $HCl(g)$  concentration) during oxidation and cooling. Lines depict the mixing ratios for species bearing the elements in question. Mixing ratios are molar ratios, corrected for the amount of the element in question in each species.

## **S6.6 Addition of [HCl] to plume**

To determine the effect of different starting chloride concentrations in the magmatic plume, the input concentration of HCl(g) was increased and decreased by three orders of magnitude above and below the measured plume composition, respectively (**Figure 8**, main text). The input compositions were the same as in **Supplementary Data S20** and outputs are in **Tables S21-27**. In the main text, the effect of changing the input concentration of HCl(g) is shown without oxidation of the plume (i.e. no mixing with ambient atmosphere). The effect of changing the input HCl(g) concentration on the speciation of the plume after the compositional discontinuity (at 25% air or  $V_A/V_M = 0.33$ ) is shown in **Supplementary Figure S13**.



**Figure S13. The effect of increasing/decreasing the chlorine content of the magmatic plume on speciation (no mixing with air).** Elements are shown in alphabetical order from top to bottom. From left to right, the input concentration (mol) of HCl(g) in the starting model is increased by an order of magnitude per column. The model result use the same input composition as in Figure 6 (Table S20) and data outputs from the altered HCl(g) models can be found in Table S21-27. Results are shown at  $V_A/V_M = 0$  or 0% mixing with ambient atmosphere. Results after the compositional discontinuity (at  $V_A/V_M = 0.33$  or 25% air) are shown in Figure 8 in the main text.

## Supplementary Note 7: Error propagation

Flow rate meter accuracy is  $\pm 5\%$  for the SKC Leland legacy pump which has a system of constant flow compensation, and was used for all size segregated results, as well as for any UAS-borne filter pack data. Flow rate meters (TSI General Purpose Thermal Mass Flowmeter Model 4034) used in conjunction with Charles Austin Capex V2 DE pumps have accuracies of  $\pm 3\%$  or  $0.1 \text{ Std L min}^{-1}$ , whichever is greater. The variability in the flow rate measured at the beginning and the end of the sampling period using the Charles Austin pump is typically greater than the quoted accuracy above, with a difference of 10% for sample FP\_8\_5, for example. Therefore a flow rate error of 10% is used for all measurements made using these pumps. During sample extraction in the lab, a main source of error is from the pipetting steps. For extraction of gas filters, 5 pipetting steps are required, each with an assumed error of  $\pm 5\%$ . For combined water and acid extractions of particulates, a total of 7 pipetting steps are required.

Instrument errors for ion chromatography (IC) are taken as the variability of the blanks for particulate and gas filters ( $\pm 8\text{-}25\%$ ). For ICP-MS and ICP-OES analysis, instrument variability (all samples were run in one batch and are therefore subject to the same instrument error) is taken into account and ranges between 10-17%, accounting for the fact that each sample is measured twice, once in the acid extraction and once in the water extraction.

Therefore for non-ash-corrected data:

$$E_{NAC} = \sqrt{(E_{icp})^2 + (E_{pip})^2 + (E_{flo})^2} \quad [2]$$

where  $E_{icp}$  is the instrument error,  $E_{pip}$  is the propagated error for all pipetting steps and  $E_{flo}$  is the flow rate error. For all element concentrations measured by ICP-MS/ICP-OES  $E_{NAC}$  is between 11-18%, for anion concentrations measured by IC,  $E_{NAC}$  is between 10-27%.

For ash corrected data, an additional error in the glass measurements is taken into account:

$$E_{AC} = \sqrt{(E_{icp})^2 + (E_{pip})^2 + (E_{flo})^2 + (E_{gls})^2} \quad [3]$$

where  $E_{ls}$  is the error in the glass analysis – here taken as either the % difference between two measurements where the data is sourced from the Fissure 8 glass analyses, the % difference between BHVO-1 and BHVO-2 ([http://georem.mpch-mainz.gwdg.de/sample\\_query\\_pref.asp](http://georem.mpch-mainz.gwdg.de/sample_query_pref.asp)) for Ag, Te, Re, B and F, and the % difference between the maximum and minimum concentrations measured in summit samples from 1971 for As and Se.

For emanation coefficients ( $\epsilon$ , see main text for equation) errors are calculated as:

$$E_{\epsilon} = \sqrt{(E_{AC})^2 + (E_{AC-S})^2 + (E_{gls})^2 + (E_{S-degassed})^2} \quad [4]$$

where  $E_{S-degassed}$  is the error on the value of  $S_{degassed}$  ( $\pm 25\%$ ),  $E_{AC-S}$  is the total concentration of sulphur measured on each sample. For ash-corrected trace elements fluxes, errors are calculated as:

$$E_{flux} = \sqrt{(E_{AC})^2 + (E_{AC-SO_2})^2 + (E_{SO_2flux})^2} \quad [5]$$

where  $E_{AC-SO_2}$  is the total concentration of  $SO_2$  gas measured on a filter pack sample and  $E_{SO_2flux}$  is the error on the  $SO_2$  flux value ( $\pm 29\%$ ).

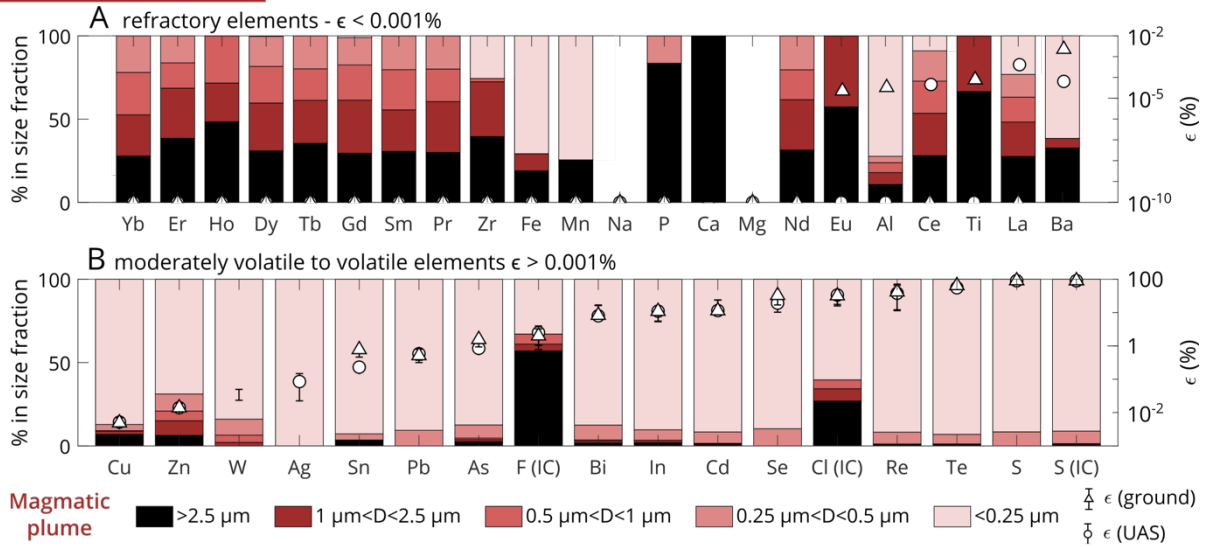
For IC data an additional source of uncertainty exists due to the effect of  $H_2O_2$  on the signal (as described in the methods). Based on experimental results<sup>1</sup>, excess  $H_2O_2$  can introduce errors for  $SO_4^{2-}$  concentrations of  $\sim 30\%$  (however we note that this may vary depending on the concentration of excess  $H_2O_2$  in the solution). Therefore we incorporate an additional error of 30% for  $SO_4^{2-}$  and  $Cl^-$  concentrations.

## Supplementary Note 8: Comparing size-segregated PM concentrations between Kīlauea's summit plume in 2008 and the LERZ eruption in 2018

Size-segregated concentrations of elements in measurements made in Kīlauea's summit plume in 2008, and those made in the plume emanating from Fissure 8 in the LERZ in 2018 in this study, show noticeable differences (**Figure S14**). Mather et al.<sup>19</sup> did not provide a detailed discussion of their size-segregated results at the time, but proposed that refractory (or lithophile) elements were predominantly found in the coarser size bins, whilst more volatile elements were found in finer size bins. As we suggest in the main text, they also suggest that the more-volatile material preferentially condenses onto the finer particles as expected for high-temperature gas-to-particle conversion<sup>20</sup>. Our size-segregated results from Kīlauea in 2018 display this distinction more clearly, and support these conclusions.

Refractory elements show similar PM size-distributions in 2008 and 2018. However, volatile elements in 2008 span a broader range of size bins in 2008, while in 2018 they are predominantly found in the smallest size bin ( $<0.25 \mu\text{m}$ ). These differences in the size-distributions of volatile elements could reflect a higher degree of particle growth between emission and sampling for the 2008 samples, as the distance between the lava lake surface and the sampling equipment is likely to have been greater in 2008 than it was in 2018. It could also reflect a lower temperature of emission, or other differences in sampling conditions.

### Kīlauea LERZ 2018



### Kīlauea summit 2009

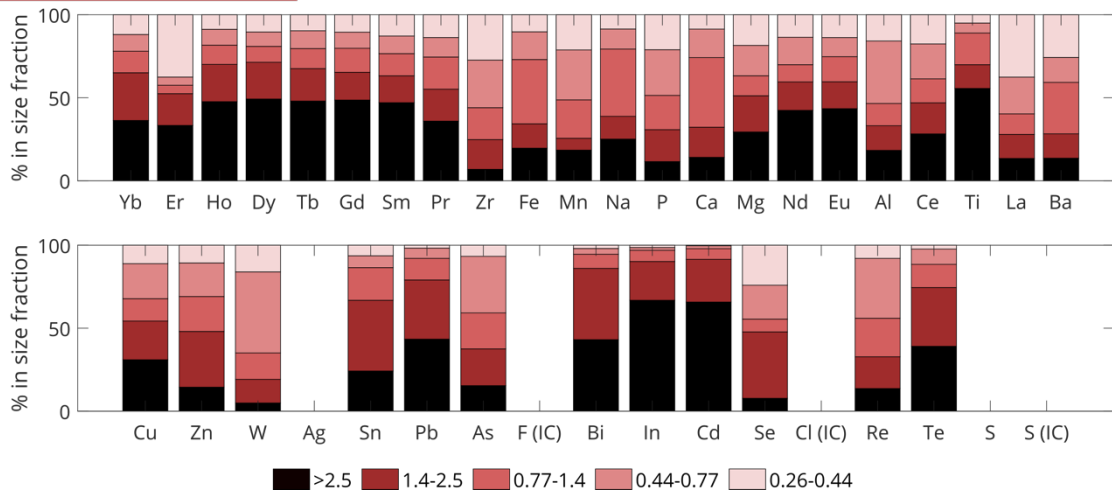


**Figure S14.** Size-segregated PM concentrations from Kīlauea's LERZ in 2018 and Kīlauea's summit emissions in 2009, plotted in the same way as in the main text for comparability. The Kīlauea 2018 concentrations are from one impactor sample in this study, while the 2009 samples are from Mather et al. (2012) and are an average of three samples from three different days in 2009.  $\epsilon$  error bars represent the propagated errors (see **Supplementary Note 7**;  $\epsilon$  data in **Supplementary Data 1 Table S10**).

## Supplementary Note 9: Estimating laze plume HCl and trace

### metal/metalloid emission rates

Estimating trace metal emission rates from the laze plume is challenging. Conventional techniques used to measure these rates in magmatic plumes (i.e., using element-to-SO<sub>2</sub> ratios and SO<sub>2</sub> emission rates, see **Error! Reference source not found.**) cannot be used due to the low SO<sub>2</sub> content of laze. To get a broad sense of trace metal emission rates from the laze plume in 2018 we follow two existing methods: **1)** Edmonds and Gerlach<sup>21</sup>, who used an estimation of how much basalt is required to boil 1 kg of seawater, and the Cl content of seawater, to estimate the HCl emission rates in a laze plume associated with lava flows emanating from the Pu'u 'Ō'ō vent (2004-05), and; **2)** Resing and Sansone (2002) who used experiments to quantify the amount of an element transferred to seawater per kilogram of lava that it comes into contact with. Both methods rely on an estimate of how much molten lava is in contact with seawater over time, which represents a large source of uncertainty. We use at-source estimates of lava effusion rates from Patrick et al.<sup>22</sup> – in late July 2018, they measured peak and trough effusion rates of 1700 and 350 m<sup>3</sup> s<sup>-1</sup>, respectively. However, the rates at which lava reaches the ocean, tens of kilometres away from the source vent, are likely to be substantially lower than this. Literature estimates for the Pu'u 'Ō'ō vent predicted that around one third of lava extruded at the vent reached the ocean<sup>23</sup>. Therefore for the 2018 eruption, to cover a range of possibilities, we assume that 30 ± 20% reached the ocean entry. At the ocean entry, only a small fraction of the molten lava gas emission rates will come into contact with seawater, which may reduce gas emission rates by 10–100 times.<sup>21</sup> This leads to the following equation:

*lava in contact with seawater (volume or mass per time)*

$$= \text{source effusion rate (volume or mass per time)} * k * c$$

Where k is the proportion of the lava extruded at source that reaches the ocean entry still-molten, and c is the proportion of this lava that then comes into ideal thermal contact with seawater. Emission rates in laze plumes are unlikely to scale linearly with lava effusion

rates, due to the lower surface area to volume ratios of larger flows, and differences in flow morphologies (e.g., pāhoehoe versus ‘a‘ā).

For **method 1** (Edmonds and Gerlach, 2006)<sup>21</sup>, we then use the quantity of lava contacting with seawater over time to calculate the amount of seawater boiled through contact with lava:

$$\text{Boiled SW (kgs}^{-1}\text{)} = \frac{\text{lava in contact with seawater (m}^3\text{s}^{-1}\text{)}}{\text{volume of lava required to boil 1kg of SW (0.001 m}^3\text{)}}$$

Assuming that seawater is boiled to dryness, they then use the Cl content of 1kg of seawater (0.1039 mol) to estimate the Cl emission rate in (mol s<sup>-1</sup>) of the laze plume:

$$\text{Cl emission rate (mols}^{-1}\text{)} = \text{Boiled SW (kgs}^{-1}\text{)} * 0.1039 \text{ mol Cl kg}^{-1}\text{SW}$$

This Cl emission rate is then converted into a trace element emission rate using X/Cl ratios in the laze plume (UAS filter pack sample 9\_2, launched from Isaac Hale Park), corrected for a silicate contribution.

For **method 2** (Resing and Sansone, 2002), we calculate trace metal/metalloid emission rates directly (i.e., without calculating a HCl emission rate first) as follows:

$$\text{Element emission rate (kgd}^{-1}\text{)} = \text{lava in contact with seawater (kgd}^{-1}\text{)} * m_x$$

Where  $m_x$  is an experimentally-derived value representing moles of an element (X) that were transferred to seawater for each kilogram of lava that it interacted with ( $m_{Cu} = 5.5 \times 10^{-7}$  moles per kg lava,  $m_{Cd} = 4.2 \times 10^{-9}$  moles per kg lava).

The results of both calculation methods for a selection of volatile metals/metalloids are given in **Supplementary Table S6**. Although the estimates cover a large range, the two methods produce similar emission rates for Cd and Cu. Notably, Cu emission rates from the ocean entry could, at times, be higher than those emitted at the main Fissure 8 vent, while other volatile metals are likely produced at much lower emission rates (**Supplementary Table S6**).

**Table S6: Comparison of metal/metalloid emission rates between the laze and magmatic plumes.** For the laze plume estimations note that the ranges represent the minimum and maximum rates based on all the parameters discussed in the main text (for minimum rate:  $k = 0.1$ ,  $c = 0.01$ , at-source effusion rate =  $350 \text{ m}^3 \text{ s}^{-1}$ ; for maximum rate:  $k = 0.5$ ,  $c = 0.1$ , at-source effusion rate =  $1700 \text{ m}^3 \text{ s}^{-1}$ ; see Methods).

Element	Laze emission rate ( $\text{kg day}^{-1}$ )		Magmatic emission rate ( $\text{kg day}^{-1}$ )	
	Edmonds and Gerlach method	Resing and Sansone method	$\text{SO}_2$ emission rate of $39 \text{ kt day}^{-1}$	max $\text{SO}_2$ emission rate of $200 \text{ kt day}^{-1}$
Cu	2.3–558	3–719	$116 \pm 30$	$593 \pm 154$
Zn	0.2–50	No data	$286 \pm 74$	$1464 \pm 381$
Cd	0.005–1.2	0.04–9.7	$296 \pm 171$	$1520 \pm 395$
Ag	0.002–0.6	No data	$0.55 \pm 0.23$	$2.8 \pm 0.7$
Bi	0.0007–0.2	No data	$23 \pm 12$	$116 \pm 30$

## Summary of supplementary data

### Supplementary Data file 1

**Data S7** – Fissure 8 concentrations

**Data S8** – Fissure 8 ash-corrected concentrations

**Data S9** – Fissure 8 size-segregated concentrations

**Data S10** – Fissure 8 volatility,  $X/\text{SO}_2$  ratios and emission rates

**Data S11** – Laze plume concentrations

**Data S12** – Laze plume ash-corrected concentrations

**Data S13** – Laze plume size-segregated concentrations

**Data S14** – Silicate glass composition used in ash correction and emanation coefficient calculation

**Data S15** – Seawater composition

**Data S16** – Global volcano comparison data for Figures 5 and 6 in the main text

**Data S17** – Fissure 8 gas compositions measured using a Multi-Gas on 24/07/18

**Data S18** – Fissure 8 gas compositions measured using a Multi-Gas on 31/07/18

**Data S19** – Blank filter compositions

### Supplementary Data file 2

**Data S20** – Magmatic plume speciation model inputs, inc.  $T$  ( $^{\circ}\text{C}$ ) and air addition

**Data S21** – Magmatic plume speciation model inputs at the measured  $[\text{HCl}(\text{g})]$

**Data S22** – Magmatic plume speciation model inputs at  $0.001 \times \text{HCl}(\text{g})$

**Data S23** – Magmatic plume speciation model inputs at  $0.01 \times \text{HCl}(\text{g})$

**Data S24** – Magmatic plume speciation model inputs at  $0.1 \times \text{HCl}(\text{g})$

**Data S25** – Magmatic plume speciation model inputs at  $10 \times \text{HCl}(\text{g})$

**Data S26** – Magmatic plume speciation model inputs at  $100 \times \text{HCl}(\text{g})$

**Data S27** – Magmatic plume speciation model inputs at  $1000 \times \text{HCl}(\text{g})$

## References

1. Wittmer, J. *et al.* Active alkaline traps to determine acidic-gas ratios in volcanic plumes: Sampling techniques and analytical methods. *Geochemistry, Geophysics, Geosystems* **15**, 2797–2820 (2014).
2. Rubin, K. Degassing of metals and metalloids from erupting seamount and mid-ocean ridge volcanoes: Observations and predictions. *Geochimica et Cosmochimica Acta* **61**, 3525–3542 (1997).
3. Gauthier, P., Sigmarsson, O., Gouhier, M., Haddadi, B. & Moune, S. Elevated gas flux and trace metal degassing from the 2014–2015 fissure eruption at the Bárðarbunga volcanic system, Iceland. *Journal of Geophysical Research: Solid Earth* **121**, 1610–1630 (2016).
4. Aiuppa, A., Dongarrà, G., Valenza, M., Federico, C. & Pecoraino, G. Degassing of Trace Volatile Metals During the 2001 Eruption of Etna. *Volcanism and the Earth's Atmosphere* (2003) doi:10.1029/139GM03.
5. Spilliaert, N., Métrich, N. & Allard, P. S–Cl–F degassing pattern of water-rich alkali basalt: Modelling and relationship with eruption styles on Mount Etna volcano. *Earth and Planetary Science Letters* **248**, 772–786 (2006).
6. Allard, P. *et al.* Acid gas and metal emission rates during long-lived basalt degassing at Stromboli Volcano. *Geophysical Research Letters* **27**, 1207–1210 (2000).
7. Bertagnini, A., Métrich, N., Landi, P. & Rosi, M. Stromboli volcano (Aeolian Archipelago, Italy): An open window on the deep-feeding system of a steady state basaltic volcano. *Journal of Geophysical Research: Solid Earth* **108**, (2003).

8. Moune, S., Gauthier, P.-J. & Delmelle, P. Trace elements in the particulate phase of the plume of Masaya Volcano, Nicaragua. *Journal of Volcanology and Geothermal Research* **193**, 232–244 (2010).
9. Moor, J. M. de *et al.* Sulfur degassing at Erta Ale (Ethiopia) and Masaya (Nicaragua) volcanoes: Implications for degassing processes and oxygen fugacities of basaltic systems. *Geochemistry, Geophysics, Geosystems* **14**, 4076–4108 (2013).
10. Allard, P. *et al.* Prodigious emission rates and magma degassing budget of major, trace and radioactive volatile species from Ambrym basaltic volcano, Vanuatu island Arc. *Journal of Volcanology and Geothermal Research* **322**, 119–143 (2016).
11. Zelenski, M. E. *et al.* Trace elements in the gas emissions from the Erta Ale volcano, Afar, Ethiopia. *Chemical Geology* **357**, 95–116 (2013).
12. Mandon, C. L., Christenson, B. W., Schipper, C. I., Seward, T. M. & Garaebiti, E. Metal transport in volcanic plumes: A case study at White Island and Yasur volcanoes. *Journal of Volcanology and Geothermal Research* **369**, 155–171 (2019).
13. Martin, R. S., Mather, T. A. & Pyle, D. M. High-temperature mixtures of magmatic and atmospheric gases. *Geochemistry, Geophysics, Geosystems* **7**, (2006).
14. Gerlach, T. M. Volcanic sources of tropospheric ozone-depleting trace gases. *Geochemistry, Geophysics, Geosystems* **5**, (2004).
15. Symonds, R. B., Reed, M. H. & Rose, W. I. Origin, speciation, and fluxes of trace-element gases at Augustine volcano, Alaska: Insights into magma degassing and fumarolic processes. *Geochimica et Cosmochimica Acta* **56**, 633–657 (1992).

16. Kress, V. C., Ghiorso, M. S. & Lastuka, C. Microsoft EXCEL spreadsheet-based program for calculating equilibrium gas speciation in the C–O–H–S–Cl–F system. *Computers & Geosciences* **30**, 211–214 (2004).
17. Gerlach, T. M. & Nordlie, B. E. The C-O-H-S gaseous system; Part II, Temperature, atomic composition, and molecular equilibria in volcanic gases. *Am J Sci* **275**, 377–394 (1975).
18. Gerlach, T. M. Oxygen buffering of Kilauea volcanic gases and the oxygen fugacity of Kilauea basalt. *Geochimica et Cosmochimica Acta* **57**, 795–814 (1993).
19. Mather, T. A. *et al.* Halogens and trace metal emissions from the ongoing 2008 summit eruption of Kīlauea volcano, Hawai‘i. *Geochimica et Cosmochimica Acta* **83**, 292–323 (2012).
20. Whitby, K. T. The Physical Characteristics of Sulfur Aerosols. in *Sulfur in the Atmosphere* (eds. Husar, R. B., Lodge, J. P. & Moore, D. J.) 135–159 (Pergamon, 1978). doi:10.1016/B978-0-08-022932-4.50018-5.
21. Edmonds, M. & Gerlach, T. M. The airborne lava–seawater interaction plume at Kīlauea Volcano, Hawai‘i. *Earth and Planetary Science Letters* **244**, 83–96 (2006).
22. Patrick, M. R. *et al.* Cyclic lava effusion during the 2018 eruption of Kīlauea Volcano. *Science* **366**, (2019).
23. Harris, A. J. L. *et al.* Calculation of lava effusion rates from Landsat TM data. *Bull Volcanol* **60**, 52–71 (1998).